Journal of Inorganic and Organometallic Polymers and Materials (2021) 31:1185–1194
https://doi.org/10.1007/s10904-020-01774-5

Comparison of Arsenate Adsorption from Neutral pH Aqueous Solutions Using Two Different Iron-Trimesate Porous Solids: Kinetics, Equilibrium Isotherms, and Synchrotron X-Ray Absorption Experiments

Eliana Berardozzi[1] · Jimena S. Tuninetti[1] · Fernando S. García Einschlag[1] · Omar Azzaroni[1] · Marcelo Ceolín[1] · Matías Rafti[1]

Received: 25 July 2020 / Accepted: 28 September 2020 / Published online: 6 October 2020

Abstract
We have explored the use of two different iron-based porous materials for arsenic uptake from neutral pH aqueous solutions. Both materials are reminiscent of a material known as MIL-100(Fe), a Metal Organic Framework (MOF) built upon the coordination of Fe(III) ions with trimesate organic linkers (benzene tricarboxylic acid). Aside from the proverbial high surface area with extended microporosity/mesoporosity, the presence of Fe(III) centers offers the possibility of specific strong interactions with arsenic, therefore making it appealing for its use in detection and purification technologies. Our approach tackles the characterization of the system from both physical and chemical perspectives. We report equilibrium isotherms and time dependent arsenic uptake for the determination of adsorption capacity and kinetics; and also, by means of synchrotron-based X-ray absorption techniques, we probe possible changes in coordination environments and oxidation states of Fe and As in the porous network occurring upon adsorption at high and low loadings. The results presented bring further insight on the nature and diversity of adsorption sites present and confirm the suitability of the proposed adsorbents for the intended use.

Keywords Fe-BTC MOFs · Arsenic removal · EXAFS/XANES · MIL-100(Fe) · Basolite F-300

1 Introduction

The presence of arsenic in ground water is an environmental, health and economical issue which affects developing countries around the world [1]. Long-term consumption of water with high arsenic-content can cause several health-threatening effects for lung, bladder, and kidney; as well as pigmentation changes, skin thickening, neurological disorders, muscular weakness, and nutritional diseases [2–4]. Arsenic excess is therefore categorized as dangerous by the World Health Organization (WHO), the USA Environmental Protection Agency (US-EPA), and the European Commission Drinking Water Directive. Accordingly, a guideline value of 10 ppb (0.01 mg/L) for the maximum allowable limit in drinking water was recently stablished [5]. However, since advanced water treatment methods needed for meeting such concentrations are both difficult to implement in rural areas and economically not feasible in many developing countries, some of those locations have retained the previous 50 ppb (0.05 mg/L) WHO limit [6]. The presence of As in groundwater and aquifers can be traced back to either natural processes (e.g., geochemical, biological, volcanic generation) or human activities (e.g., fossil fuels combustion, mining, or the use of wood preservatives and agricultural pesticides) [7, 8]. For example, all along the Chaco-Pampeana plain in Argentina ($\approx 10^6$ km^2), arsenic concentrations in

Electronic supplementary material The online version of this article (https://doi.org/10.1007/s10904-020-01774-5) contains supplementary material, which is available to authorized users.

✉ Marcelo Ceolín
mceolin@inifta.unlp.edu.ar

✉ Matías Rafti
mrafti@quimica.unlp.edu.ar

[1] Facultad de Ciencias Exactas, Departamento de Química, Instituto de Investigaciones Fisicoquímicas Teóricas y Aplicadas (INIFTA), Universidad Nacional de La Plata (UNLP), CONICET, La Plata 1900, Argentina

water can be as high as 300 ppb due to natural geogenic processes posing a serious threat for health and demanding the application of specific public policies. Several strategies for diminishing arsenic content in drinking water were recently proposed, and some were already implemented in both, pilot and large-scale treating facilities [9]. Arsenic can be present as As(III) or As(V) depending on the reservoir conditions (anoxic or oxic respectively); adsorption of arsenate (As(V)) species is substantially more efficient and therefore different strategies for pre-oxidation steps were reported extensively [10, 11]. Mechanisms underlying arsenic removal depend strongly on several process parameters, as well as on the specific interactions with selected adsorbents; one of the most interesting examples in this regard are iron oxyhydroxides [12, 13]. The origin of specific interactions between iron-based adsorbents and arsenate species can be traced back to the formation of relatively strong inner-sphere complexes on ferrihydrite moieties, acting as specific adsorption sites [14–18]. Despite their low cost and wide availability, the use of many natural iron oxides sorbents suffers from low loading capacities and sluggish kinetics related to small specific surface areas, in addition to non-straightforward regeneration procedures, a key feature when aiming for its application in continuous processes [19]. Triggered by the above discussed shortcomings, a different approach was recently explored for water remediation treatments in general, and arsenic removal technologies in particular; i.e., the use of metal organic frameworks (MOFs) as high-performance adsorbents. MOFs can be described as three-dimensional porous networks constituted by metal ions (or clusters containing metal ions) acting as coordination centers, non-covalently bonded with multidentate organic linkers [20–24]. The judicious choice of metal and linker allows for a great structural versatility, while via e.g., post-synthetic modification, further fine tuning of key properties such as porosity, morphology, and surface chemistry is possible [25, 26]. Various Al- and Fe-based MOFs have been recently tested for arsenic removal, although the use of Fe-MOFs (due to its biocompatibility and metal precursor availability) [27] is much more appealing, considering the hazardous nature of Al(III) ions, which impose additional constraints for its use [24, 28, 29]. Remarkably, examples of Fe-MOFs featuring permanent porosity, water stability, and high surface areas were few until 2007, when MIL-100(Fe) (acronym from Matériaux de l'Institute Lavoisier) was first reported [30]. Following such milestone, several studies highlighting multiple applications appeared [31–33]; and specifically, given the different adsorption sites available [30, 34], its use as a versatile heterogeneous catalysts was extensively reported [35–37]. Even BASF chemical company made available a series of porous materials ("Basolites"), including a Fe-BTC porous material (BTC = benzene tricarboxylic acid, or trimesic acid) commercialized as Basolite F-300 which features a structure closely related to MIL-100(Fe) MOF but with lower crystallinity. MIL-100(Fe) structure can be described as supertetrahedra built from trimers of FeO_6 octahedra bridged by shared μ_3-O which delimits two types of cages (namely, 5 Å pentagonal, and 8.6 Å hexagonal), see Scheme 1.

Fundamental differences between Basolite F-300 and MIL-100(Fe) regarding surface area and catalytic activity can be attributed to structural variations causing modifications on the number of available Lewis acid or redox active sites present [39]. Redox activity stems from coordinatively unsaturated metal sites (Fe-CUS), and endows the resulting porous material with the interesting possibility of selective adsorption [40, 41]. Aside from structural defects present in F-300, differences observed were also hypothesized to arise from the presence of some residual amount of Fe(II) in the porous matrix. Recent studies using composite materials which combine Fe-BTC and polymers showed promising performances for As(V) adsorption, although further insight is need for a detailed understanding on the mechanism operating and the changes occurring in atomic coordination environments occurring upon adsorption [42].

Inspired by the above discussed ideas, we have herein conducted experiments oriented to evaluate the feasibility of using commercially available Fe-based porous materials for arsenic adsorption from aqueous solutions at neutral pH. In order to gain further insight on the adsorption mechanism, we carried experiments for arsenic determination in the matrix using both surface sensitive (X-Ray Photoelectric Spectroscopy, XPS) and bulk averaged (inductively coupled

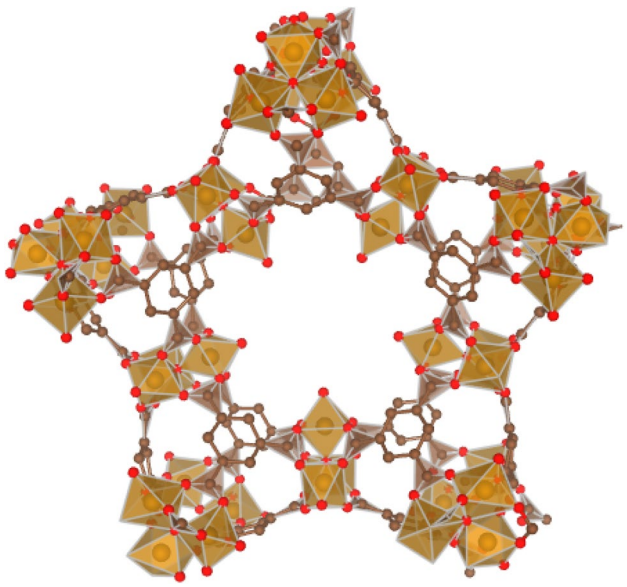

Scheme 1 MIL-100(Fe) pentagonal cage (pore aperture ≈ 5 Å) with structure building units and μ_3-O-linked FeO_6-octahedra (produced with VESTA [38] software)

plasma atomic emission spectroscopy, ICP-AES) techniques on both commercial (BASF F-300), and synthesized (Fe-BTC produced with environmentally-friendly hydrofluoric acid-free (HF) procedure) Fe-based porous solids [43, 44]. Although Mössbauer spectroscopy is commonly employed for assessing structural changes on Fe-containing solids during synthesis and after exposure to different operating conditions (including adsorption processes); we aim to gain further insight by using synchrotron-based X-Ray adsorption techniques, such as extended X-Ray absorption fine structure (EXAFS) and X-Ray absorption near edge structure (XANES). Inspired by recently published examples in which EXAFS/XANES techniques were employed as a tool for determination of the influence of exposure to aqueous environments on structure and catalytic activity of Fe-based adsorbents [45–47], we have assessed the occurrence of structural modifications on the porous matrix induced by different As-loadings. [48] Moreover, we have explored the possibility of charge-transfer between Fe(III) and As(V) during adsorption by comparing results obtained with appropriate standards.

2 Experimental

2.1 Chemicals

H_3BTC, Benzene-1,3,5-tricarboxylic acid $C_6H_3(CO_2H)_3$ was purchased from Sigma Aldrich, ferric sulfate $Fe_2(SO_4)_3.9H_2O$ was provided by Mallinkrodt, analytic grade sodium arsenate $Na_2HAsO_4.7H_2O$, ascorbic acid $C_6H_8O_6$, ammonium molybdate $Mo_7O_{24}(NH_4)_6.4H_2O$, potassium antimonil tartrate $Sb_2C_8H_4K_2O_{12}.3H_2O$ and sulfuric acid 98% H_2SO_4 were provided by Anedra and used as received without further purification. The solutions were prepared using Milli-Q grade water (Millipore).

2.2 Synthesis

Basolite F-300 was used as purchased from BASF. Fe-BTC MOF was synthesized according to published methods with slight modifications [43]. Briefly, the procedure followed avoids the use of highly corrosive HF, commonly employed as mineralizing agent, and involves hydrothermal reaction of aqueous solutions of ferric sulfate and H_3BTC precursors, and kept for 12 h at 160 °C under autogenous pressure in Teflon-lined stainless-steel reactors (molar ratio of ($Fe_2(SO_4)_3$:H_3BTC:H_2O) precursors (1:0.67:280)).

2.3 Methods

All tests presented in this study were carried out in batch systems kept at room temperature (25 °C). To perform the experiments, 250 mL beakers covered with aluminum foils were used as reactors. Solutions used were prepared from stock solutions of As(V) as arsenate (AsO_4^{3-}) 500.0 ppm concentration, and pH = 7.0 was adjusted using either HCl or NaOH 0.1 N solutions. Appropriate homogeneity of the system was ensured by continuous magnetic stirring throughout experiments. When contact time was elapsed (48 h, see below), adsorbent was separated from the solutions using 0.45 µm nylon syringe filters and washed thoroughly with fresh solvent. For the equilibrium and kinetic experiments, arsenic concentrations were determined *via* the Mo-blue assay; briefly, it makes use of the arsenic reaction occurring in presence of ascorbic acid and ammonium molybdate, which yields a colored antimonil-arsenomolybdate complex with a color intensity proportional to arsenic concentration that can be determined with spectrophotometric methods (see ESI for further details on equations used for adsorption isotherms and fitting procedures) [49, 50].

2.4 Equilibrium Adsorption Isotherms and Adsorption Kinetics

Langmuir and Freundlich isotherms are among the most used models for describing adsorption equilibrium, and although relatively simplistic, parameters extracted from appropriate fitting of experimental data allow for meaningful comparison between different materials [51–53]. Batch experiments were conducted in order to determine the contact time required to reach adsorption equilibrium, and data was evaluated using different kinetic models (e.g., pseudo-first- and second-order) [51, 52]. Adsorption experiments were carried using different initial arsenate concentrations ranging from 0.1 to 80 mg/L with an adsorbent dose of 45.0 mg/L, at 25 °C for 48 h with fixed pH = 7.0 (see ESI for further details).

2.5 Structural and Morphological Characterization of Materials Employed

Chemical insight on the presence and concentration of arsenic in the porous solid was obtained using vibrational spectroscopy (FTIR), X-Ray Photoelectron Spectroscopy (XPS), Ion Coupled Plasma Spectroscopy. EXAFS/XANES experiments were carried at the D08B-XAFS2 beam line of the Laboratório Nacional de Luz Síncrotron (CNPEM-LNLS, Campinas, Brazil). Spectra pre-processing, and model fitting and scattering path calculation was done using the routines coded in the DEMETER suite [54]. Thermogravimetric Analysis (TGA), X-Ray diffraction experiments and Transmission Electronic Microscopy were conducted in order to structurally characterize the materials used and the effect of arsenic exposure (see ESI for further details).

Table 1 Kinetic parameters obtained by fitting the experimental profiles with both the pseudo-first and pseudo-second order models

F-300 load	Pseudo-first order		Pseudo-second order	
400 mg/L	k_1	2.539	k_2	52.802
	R^2	0.75	R^2	1
100 mg/L	k_1	0.669	k_2	0.584
	R^2	0.993	R^2	0.998
16 mg/L	k_1	0.147	k_2	0.008
	R^2	1	R^2	1

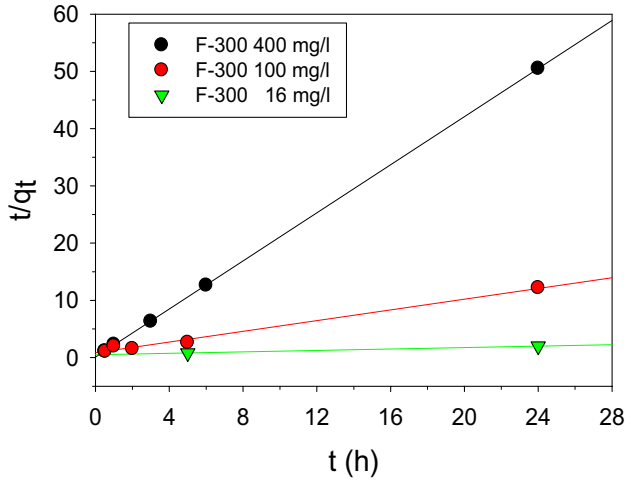

Fig. 1 Pseudo second order fit for the time evolution using As(V) adsorption with 400, 100 and 16 mg/L F-300 adsorbent dose.

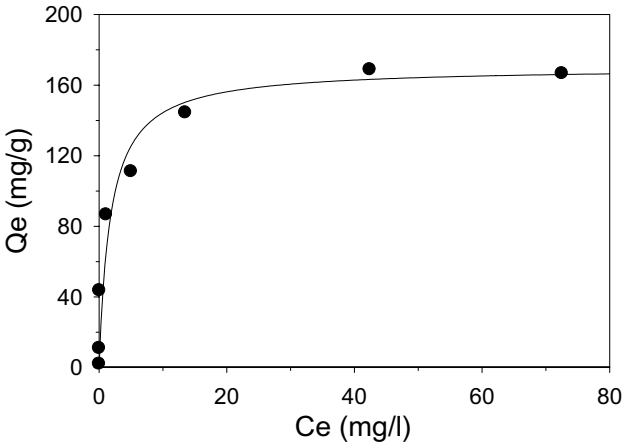

Fig. 2 Experimental determination of adsorption isotherm together with Langmuir fit (solid line), conditions used: 25 °C, pH = 7.0, and F-300 adsorbent dose 45 mg/L

Table 2 Equilibrium parameters obtained by fitting the experimental data with Langmuir and Freundlich model isotherms for adsorption on F-300

Langmuir		Freundlich	
K_L	1.031 L/mg	K_F	53.85 mg/g
q_m	169.2 mg/g	N	1.43
R^2	0.9983	R^2	0.8095

3 Results and Discussion

3.1 Adsorption Isotherms and Kinetics of As(V) Adsorption on F-300 Porous Matrix

In order to determine suitable equilibration times for adsorption process, time evolution of As(V) concentration was followed and different kinetic models were applied. Table 1 shows the kinetic parameters obtained by fitting the experimental data with both, pseudo-first and pseudo-second order models. The effect of adsorbent amount used on adsorption kinetics was evaluated using 200 ppb of initial As(V) concentration with F-300 solid doses of 400, 100 and 16 mg/L. Figure 1 depicts the pseudo-second order fit obtained for time evolution for As(V) concentration, which was observed to represent better the underlying process (see FTIR vibrational bands associated to the presence of Arsenic in the porous matrix shown in Fig. 1S, ESI). It should be emphasized that, although specific characteristics of the system make it very complex, a quite simple kinetic model is capable of providing a relatively good fit (see ESI for further details).

Having determined appropriate contact times for equilibration and adsorbent dose, we proceeded to measure As(V) adsorption isotherms (see Fig. 2), which were then modeled using both Langmuir and Freundlich models. Model parameters obtained from fitting are summarized in Table 2.

According to Langmuir fitting parameters obtained, maximum arsenic load can be calculated to be 169.2 mg g^{-1} (corresponding to an As/Fe ratio of 0.794), and considering 2 coordinatively unsaturated sites (CUS) per Fe_3O trimer, a value of 0.74 arsenate per CUS. The obtained results are in line with recent reports for As adsorption using Fe/Mg-MIL-88B (featuring an uptake of about 300 mg g^{-1}) [55], or MIL-100(Fe) in which maximum load and number of arsenate adsorbed per CUS were 124 mg g^{-1} and 0.54 respectively [56], constituting a remarkably high value compared with other adsorbent materials (see Table S1 in the ESI). It should be stressed that Zr-based UiO-66 MOF was recently reported to reach loadings as high as 303.3 mg g^{-1}, although in order to attain such values non-neutral conditions are needed [57].

3.2 Comparison of Arsenic Content on F-300 Adsorbent Using Surface Sensitive (XPS) and Bulk Averaged (ICP) Detection Techniques

The study of significant differences between Arsenic content (or As/Fe ratio) when determined using surface sensitive techniques (XPS, with few nanometers penetration depth) or bulk-averaged techniques (ICP, applied after chemical digestion of dried samples, see Experimental section), allows gaining additional insight on the adsorption process. In other words, if the porous matrix features identical homogeneously distributed sites, the determined equilibrium As/Fe ratio should not differ regardless the technique used (i.e., significant differences would suggest the existence of inhomogeneities). Table 3 shows values obtained for As/Fe ratio as determined with XPS or ICP.

Remarkably in line with the above discussed adsorption experiments, in which the As/Fe ratio was determined to be 0.794 (as derived from extrapolation using Langmuir adsorption model), ICP derived value was 0.761. The value of 0.415 obtained from XPS is somehow lower, thus suggesting a degree of heterogeneity which would render lower arsenic surface concentrations. In order to bring further insight to this issue and to determine whether such difference can be considered significant, we have conducted synchrotron-light X-Ray absorption experiments (see discussion below, section 3.5 for EXAFS and XANES experiments).

3.3 Structural Characterization of Materials used and the Effect of Exposure to Arsenic

Wide Angle X-Ray Scattering (WAXS) experiments were carried on powder samples, diffractograms corresponding to F-300 before and after exposure to As(V) aqueous solutions are presented in Fig. 3 together with calculated diffractogram from reported MIL-100(Fe) structure (see the results shown as ESI for benchmark Fe-BTC synthesized material after exposure to As(V), Fig. S2 and TEM images in Fig. S3 where octahedral morphology can be observed) [30]. It can be inferred from the diffractograms obtained that no additional crystallinity loss occurs after exposure to As(V) [58].

Table 3 ICP and XPS As/Fe ratio determination for Fe-300 adsorbent exposed to high As(V) concentration after reaching equilibrium

	ICP			XPS	
	Concentration (mg As per g sample)	Concentration (mg Fe per g sample)	As/Fe	Atomic % (As /Fe)	As/Fe
F-300/ As(V) saturation	273.63	320.33	0.761	0.31	0.415

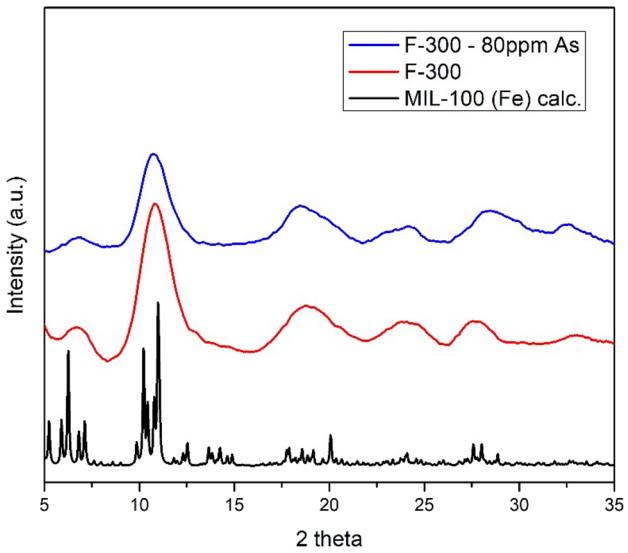

Fig. 3 Comparison between diffraction patterns obtained for F-300 porous solid, both after and before exposure to 80 ppm As(V) aqueous solutions, versus MIL-100(Fe)

3.4 Thermal Stability of the Bare Porous Adsorbent and the Effect of Arsenic Loadings Studied via TGA

Figure 4 displays TGA experiments in which thermal stability of both F-300 and Fe-BTC solids are compared, N_2 atmosphere and 10 K/min heating ramps were used. In line with recent reports, decomposition profiles observed for both materials feature two stages of weight loss (wl_i); namely, initial events centered around 350 °C (wl_1) followed by events centered at 450 °C (wl_2). The value for the ratio for such weight losses ($r = wl_1/wl_2$) can be used to characterize the composition of materials; e.g., it was observed to be approximately $r = 1.5$ for highly crystalline MIL-100(Fe), while it can be as high as 2.2 if significant amounts of unreacted organic linker (BTC) remain present (this fact can be understood by considering that H_3BTC decomposition thermal event is rather abrupt and starts at ≈ 300 °C) [44]. Determined values for the weight loss ratio were $r_{\text{F-300}} = 1.11$ and $r_{\text{Fe-BTC}} = 2.27$; while the relatively low value for commercial F-300 might be related to purification procedures and/or excess of metal precursor, the value obtained for synthesized Fe-BTC is well within recent reported values for similar synthesis procedures, and can be rationalized in terms of an excess of unreacted organic linker present the porous matrix.

Having studied the thermal profiles of porous materials used, we further explored the effect of As(V) adsorption.

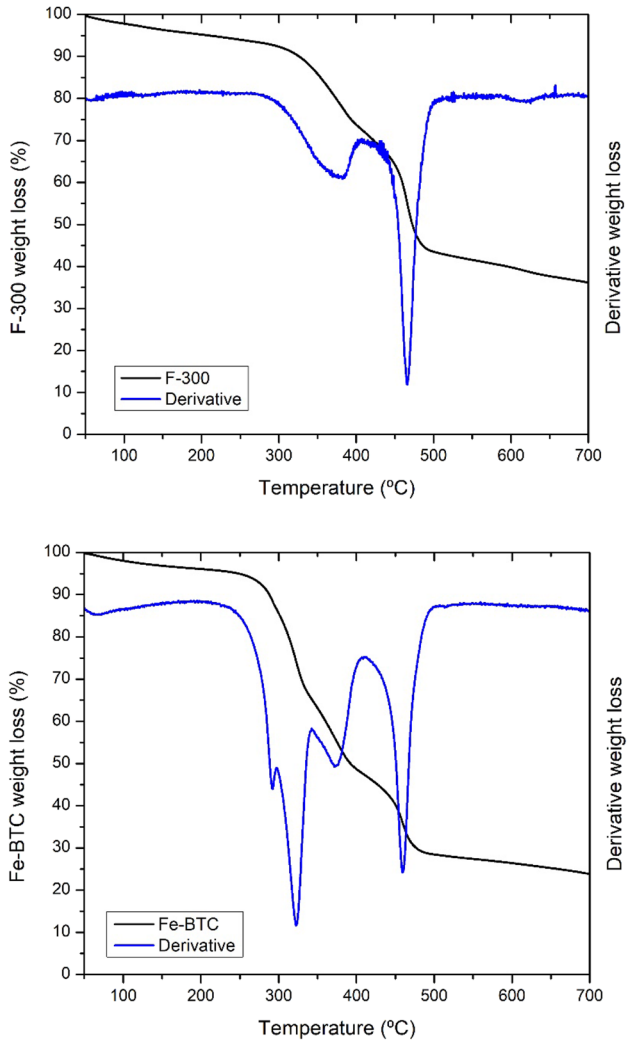

Fig. 4 Thermal decomposition profiles for: (top) Fe-300 and (bottom) benchmark Fe-BTC bare porous materials

Thermal events corresponding to bare As(V) occur quite early in temperature (160 °C) and thus can be deconvoluted from those corresponding to Fe-trimesate porous solids, however, increasing loadings of Arsenic can be detected via TGA by following the increase in residual material at final temperatures (see Fig. S7 in ESI).

3.5 X-Ray Absorption Experiments for Determination of Arsenic and Iron Atomic Environments and Oxidation States on the Porous Matrix Under for Different Loadings

Having established the presence of Arsenic in the porous adsorbent after exposure, and considering differences observed between XPS- and ICP-determined As/Fe ratio (i.e., using either a surface confined or a volume averaged technique, see sec. 3.2 above); it remains the question of whether adsorption sites available can be thought as homogeneously distributed or not; both regarding an spatial and energetic perspective. Synchrotron-light based EXAFS and XANES experiments were carried to gain insight in this regard using both F-300 and Fe-BTC benchmark dried powder samples after exposure to Arsenic aqueous solutions. Additionally, another interesting question that can be answer by resorting to X-Ray absorption techniques concerns the possibility of redox process occurring during adsorption. Fe-based porous solids contain Fe(III) (aside from minor Fe(II) impurities that might be present); while adsorbed Arsenic species were introduced as As(V) oxyanion; however, it might be hypothesized that adsorption processes occur together with charge transfer up to some extent. Iron acetate, as Fe(III) reference structure, was used as starting point to model Fe local environments in the porous solids [45], while Arsenic environments were modelled using metamunirite-like local environments (see Scheme S1 in the ESI) [59]. Arsenic K-edge XANES experiments corresponding to reference materials featuring As(III) and As(V) oxidation states, and both F-300 and Fe-BTC after exposure to 80 ppm As(V) stock solutions were compared (see Figure S5 in the ESI). It is clear that no As(III) is present on the adsorbed phase, thus ruling out the possibility of adsorptive reduction, as both Fe-BTC and F-300 samples feature peaks centered virtually at the same energy values. The EXAFS signals obtained for Arsenic in both F-300 and Fe-BTC porous materials can be observed in Figure S6 (ESI).

EXAFS results obtained were successfully modelled by using two single-scattering paths and two multiple-scattering paths. Derived Arsenic-Oxygen scattering paths and O–As–O bond angles are shown in Table 4, in both cases only As(V) oxidation state is considered. Although scattering paths obtained for Arsenic-Oxygen remain virtually unchanged when comparing adsorbed As(V) on the porous materials and model metamunirite mineral; As–O–As bond angles variate significantly, suggesting interactions between As(V) oxoacid species and carboxylate exposed moieties in the porous support as previously proposed (see also Figure S1 in ESI for further details derived from vibrational spectroscopy) [57].

Iron K-edge XANES experimental data obtained was compared with different iron standards; both shape and position of pre-edge features observed agree well with Fe(III) signal, thus ruling out the presence of any amount of reduced Fe(II) CUS on the porous solids (neither resulting from synthesis procedure, nor caused by exposure to aqueous environments or Arsenic adsorption, see Fig. 5). Moreover, XANES results obtained show no structural effects attributable to increasingly higher Arsenic loads on the porous network (see ESI figure S4). Features observed can be assimilated to a Fe(III) local

Table 4 Scattering paths needed (Angstroms) for modelling results obtained as well as bond angles for Arsenic standard and Fe-based porous materials loaded with 80 ppm As(V) solutions

Sample	d (As-O1)	d (As-O2)	∀ O1-As-O2
Metamunirite As(V) standard	1.727	1.665	144
80 ppm As(V) Fe-BTC	1.723	1.661	136
80 ppm As(V) F-300	1.725	1.662	136

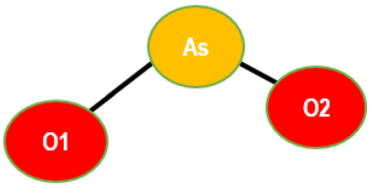

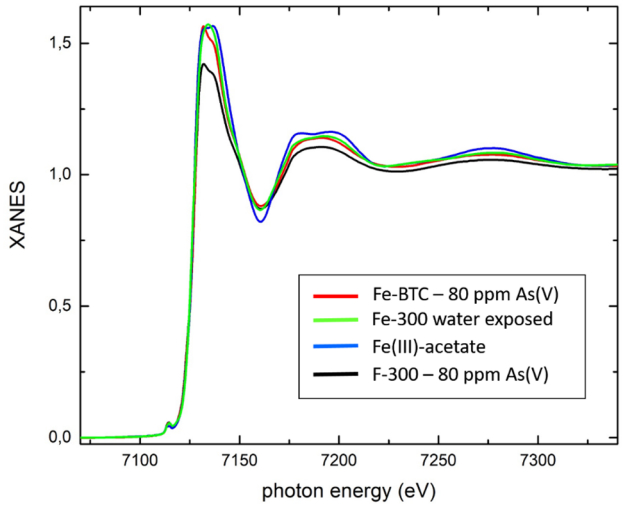

Fig. 5 Iron K-edge XANES experiments carried over Fe-BTC and F-300 porous materials loaded with 80 ppm As(V) solutions, together with a comparison versus ferric acetate standard

environment indistinguishable from iron acetate standard used, see Table 5 for details on scattering paths considered and values obtained from modelling. It is important to stress the fact that exposure to aqueous environments causes no detectable changes on the XANES experimental response, which remain fixed in what can be expected for the Fe(III) acetate local environments, in line with discussed X-ray diffraction results.

4 Conclusions

We have presented a detailed analysis of arsenate adsorption on Fe-trimesate porous solids using neutral aqueous solutions. Structural modifications occurring in both commercial F-300 and laboratory synthesized Fe-BTC porous solids were compared with multiple techniques such as synchrotron-based X-Ray absorption, vibrational spectroscopy, thermogravimetry, XPS and ICP. Adsorbents were demonstrated to remain structurally stable upon exposure to aqueous environments and adsorption in high and low loading limit. Direct interaction of arsenate oxyanions and Fe-based adsorbent sites was demonstrated by synchrotron X-Ray adsorption experiments. Specifically, we were able to determine the absence of either total or partial charge-transfer processes upon arsenate adsorption (i.e., retention of Fe(III) and As(V) oxidation states); by comparing results obtained using high and low arsenate loadings on the porous solid, the hypothesis of energetically non-homogeneous adsorption sites can be discarded. Such finding is line with the observation of Langmuir isotherm model (which assumes homogeneously distributed adsorption sites) to be more appropriate for interpretation of adsorption experiments than Freundlich isotherm model. Coordination environments determined for both F-300 and Fe-BTC porous matrixes are compatible with what can be expected for Fe(III) acetate-model structure employed, with no evidence of modifications caused by aqueous environments, as suggested also by WAXS experimental results. Moreover, no specific structural differences were observed when comparing F-300 and benchmark Fe-BTC (aside from a slight

Table 5 Scattering paths (Angstroms) needed for modelling results obtained using iron (III) acetate standard and Fe-based porous materials loaded with 80 ppm As(V) solutions

Sample	d (Fe-O13)	d (Fe-O1)	d Fe-O3
Iron (III) acetate standard	1.897	1.995	2.063
80 ppm As(V) Fe-BTC	1.897	1.992	2.112
80 ppm As(V) F-300	1.899	1.986	2.081

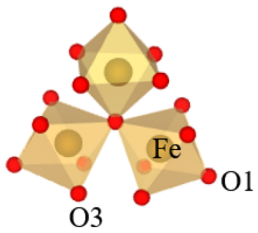

linker excess for Fe-BTC, as determined by TGA weight loss event ratios). Taking into account the low crystallinity as evidenced by WAXS together with above discussed EXAFS results, porous matrixes used can be regarded as an overall disordered porous network with short range locally ordered Fe-acetate units. Despite the low crystallinity caused by the modified synthesis procedure, remarkably high As uptakes were obtained (as high as 162 mg g^{-1}) with equilibration periods suitable for practical applications; even comparable with performances reported using high crystallinity MIL-100(Fe) [56]. The hereby reported results suggest that substantial improvement is still possible for the (already quite successful) [11] application of novel and cost-effective Fe-based porous materials for As removal.

Acknowledgements J.S.T., F.S.G.E., O.A., M.C., and M.R. are CONICET fellows and like to acknowledge the Agencia Nacional de Promoción Científica y Tecnológica (ANPyCT, projects PICT-2014-0463 and PICT-2018-00780) for financial support. E.B gratefully acknowledges CONICET for the scholarship granted. The SAXS/WAXS system (INIFTA, project "Nanopymes", EuropeAid/132184/D/SUP/AR-Contract 331−896). Laboratório Nacional de Luz Síncrotron is gratefully acknowledged for funding granted related to experiments carried in Campinas, SP, Brasil.

Funding Funding was provided by Fondo para la Investigación Científica y Tecnológica and Consejo Nacional de Investigaciones Científicas y Técnicas.

Reference

1. Z. Wang, H. Guo, W. Xiu, J. Wang, M. Shen, High arsenic groundwater in the Guide basin, northwestern China: distribution and genesis mechanisms. Sci. Total Environ. **640–641**, 194–206 (2018)
2. H.-F. Chiu, S.-C. Ho, L.-Y. Wang, T.-N. Wu, C.-Y. Yang, Does arsenic exposure increase the risk for liver cancer? J. Toxicol. Environ. Heal. Part A **67**, 1491–1500 (2004)
3. O.F. Brouwer, W. Onkenhout, P.M. Edelbroek, J.F.M. de Kom, F.A. de Wolff, A.C.B. Peters, Increased neurotoxicity of arsenic in methylenetetrahydrofolate reductase deficiency. Clin. Neurol. Neurosurg. **94**, 307–310 (1992)
4. C. Hopenhayn-Rich, M.L. Biggs, A. Fuchs, R. Bergoglio, E.E. Tello, H. Nicolli, A.H. Smith, Bladder cancer mortality associated with arsenic in drinking water in argentina. Epidemiology **7**, 117–124 (1996)
5. J.T. Kretchik, *Arsenic in Drinking Water*, National Academies Press, Washington, D.C., 1999, vol. 9.
6. R. Quansah, F.A. Armah, D.K. Essumang, I. Luginaah, E. Clarke, K. Marfoh, S.J. Cobbina, E. Nketiah-Amponsah, P.B. Namujju, S. Obiri, M. Dzodzomenyo, Association of arsenic with adverse pregnancy outcomes/infant mortality: a systematic review and meta-analysis. Environ. Health Perspect. **123**, 412–421 (2015)
7. D. Mohan, C.U. Pittman, Arsenic removal from water/wastewater using adsorbents-A critical review. J. Hazard. Mater. **142**, 1–53 (2007)
8. M.I. Litter, A.M. Ingallinella, V. Olmos, M. Savio, G. Difeo, L. Botto, E.M. Farfán Torres, S. Taylor, S. Frangie, J. Herkovits, I. Schalamuk, M.J. González, E. Berardozzi, F.S. García Einschlag, P. Bhattacharya, A. Ahmad, Arsenic in Argentina: occurrence, human health, legislation and determination. Sci. Total. Environ. **676**, 756–766 (2019)
9. M.I. Litter, A.M. Ingallinella, V. Olmos, M. Savio, G. Difeo, L. Botto, E. Mónica, F. Torres, S. Taylor, S. Frangie, J. Herkovits, I. Schalamuk, M. José, E. Berardozzi, F.S. García, P. Bhattacharya, A. Ahmad, Science of the total environment arsenic in argentina : technologies for arsenic removal from groundwa- ter sources, investment costs and waste management practices. Sci. Total Environ. **690**, 778–789 (2019)
10. M.C. Dodd, N.D. Vu, A. Ammann, V.C. Le, R. Kissner, H.V. Pham, T.H. Cao, M. Berg, U. Von Gunten, Kinetics and mechanistic aspects of As(III) oxidation by aqueous chlorine, chloramines, and ozone: Relevance to drinking water treatment. Environ. Sci. Technol. **40**, 3285–3292 (2006)
11. D. Wang, S.E. Gilliland, X. Yi, K. Logan, D.R. Heitger, H.R. Lucas, W.-N. Wang, Iron mesh-based metal organic framework filter for efficient arsenic removal. Environ. Sci. Technol. **52**, 4275–4284 (2018)
12. H. Guo, D. Stüben, Z. Berner, Removal of arsenic from aqueous solution by natural siderite and hematite. Appl. Geochemistr. **22**, 1039–1051 (2007)
13. W. Zhang, P. Singh, E. Paling, S. Delides, Arsenic removal from contaminated water by natural iron ores. Miner. Eng. **17**, 517–524 (2004)
14. G.A. Waychunas, C.C. Fuller, B.A. Rea, J.A. Davis, Wide angle X-ray scattering (WAXS) study of "two-line" ferrihydrite structure: effect of arsenate sorption and counterion variation and comparison with EXAFS results. Geochim. Cosmochim. Acta **60**, 1765–1781 (1996)
15. B.A. Manning, S.E. Fendorf, S. Goldberg, Surface Structures and Stability of Arsenic(III) on Goethite: Spectroscopic Evidence for Inner-Sphere Complexes. Environ. Sci. Technol. **32**, 2383–2388 (1998)
16. S. Mandal, M.K. Sahu, R.K. Patel, Adsorption studies of arsenic(III) removal from water by zirconium polyacrylamide hybrid material (ZrPACM-43). Water Resour. Ind. **4**, 51–67 (2013)
17. S. Yao, Z. Liu, Z. Shi, Arsenic removal from aqueous solutions by adsorption onto iron oxide/activated carbon magnetic composite. J. Environ. Heal. Sci. Eng. **12**, 1–8 (2014)
18. S. Goldberg, C.T. Johnston, Mechanisms of arsenic adsorption on amorphous oxides evaluated using macroscopic measurements, vibrational spectroscopy, and surface complexation modeling. J. Colloid Interface Sci. **234**, 204–216 (2001)
19. R. Singh, S. Singh, P. Parihar, V.P. Singh, S.M. Prasad, Arsenic contamination, consequences and remediation techniques: a review. Ecotoxicol. Environ. Saf. **112**, 247–270 (2015)
20. E.M. Dias, C. Petit, Towards the use of metal-organic frameworks for water reuse: a review of the recent advances in the field of organic pollutants removal and degradation and the next steps in the field. J. Mater. Chem. A **3**, 22484–22506 (2015)
21. J.L.C. Rowsell, O.M. Yaghi, Metal–organic frameworks: a new class of porous materials. Microporous Mesoporous Mater. **73**, 3–14 (2004)
22. G. Férey, Hybrid porous solids: past, present, future. Chem. Soc. Rev. **37**, 191–214 (2008)
23. L.E. Kreno, K. Leong, O.K. Farha, M. Allendorf, R.P. Van Duyne, J.T. Hupp, Metal-organic framework materials as chemical sensors. Chem. Rev. **112**, 1105–1125 (2012)
24. S. Hou, Y.N. Wu, L. Feng, W. Chen, Y. Wang, C. Morlay, F. Li, Green synthesis and evaluation of an iron-based metal-organic framework MIL-88B for efficient decontamination of arsenate from water. Dalt. Trans. **47**, 2222–2231 (2018)
25. S.M. Cohen, Postsynthetic methods for the functionalization of metal-organic frameworks. Chem. Rev. **112**, 970–1000 (2012)

26. S. Yuan, L. Feng, K. Wang, J. Pang, M. Bosch, C. Lollar, Y. Sun, J. Qin, X. Yang, P. Zhang, Q. Wang, L. Zou, Y. Zhang, L. Zhang, Y. Fang, J. Li, H.C. Zhou, Stable metal-organic frameworks: design, synthesis, and applications. Adv. Mater. **30**, 1–35 (2018)
27. T. Baati, L. Njim, F. Neffati, A. Kerkeni, M. Bouttemi, R. Gref, M.F. Najjar, A. Zakhama, P. Couvreur, C. Serre, P. Horcajada, In depth analysis of the in vivo toxicity of nanoparticles of porous iron(iii) metal–organic frameworks. Chem. Sci. **4**, 1597–1607 (2013)
28. C. Chen, M. Zhang, Q. Guan, W. Li, Kinetic and thermodynamic studies on the adsorption of xylenol orange onto MIL-101(Cr). Chem. Eng. J. **183**, 60–67 (2012)
29. J. Cai, X. Wang, Y. Zhou, L. Jiang, C. Wang, Selective adsorption of arsenate and the reversible structure transformation of the mesoporous metal-organic framework MIL-100(Fe). Phys. Chem. Chem. Phys. **18**, 10864–10867 (2016)
30. P. Horcajada, S. Surblé, C. Serre, D.Y. Hong, Y.K. Seo, J.S. Chang, J.M. Grenèche, I. Margiolaki, G. Férey, Synthesis and catalytic properties of MIL-100(Fe), an iron(III) carboxylate with large pores. Chem. Commun. **100**, 2820–2822 (2007)
31. R. Anand, F. Borghi, F. Manoli, I. Manet, V. Agostoni, P. Reschiglian, R. Gref, S. Monti, Host-guest interactions in Fe(III)-trimesate MOF nanoparticles loaded with doxorubicin. J. Phys. Chem. B **118**, 8532–8539 (2014)
32. A. Zimpel, T. Preiß, R. Röder, H. Engelke, M. Ingrisch, M. Peller, J.O. Rädler, E. Wagner, T. Bein, U. Lächelt, S. Wuttke, Imparting Functionality to MOF Nanoparticles by External Surface Selective Covalent Attachment of Polymers. Chem. Mater. **28**, 3318–3326 (2016)
33. D. Wang, M. Wang, Z. Li, Fe-based metal-organic frameworks for highly selective photocatalytic benzene hydroxylation to phenol. ACS Catal. **5**, 6852–6857 (2015)
34. P. Horcajada, H. Chevreau, D. Heurtaux, F. Benyettou, F. Salles, T. Devic, A. Garcia-Marquez, C. Yu, H. Lavrard, C.L. Dutson, E. Magnier, G. Maurin, E. Elkaïm, C. Serre, Extended and functionalized porous iron(iii) tri- or dicarboxylates with MIL-100/101 topologies. Chem. Commun. **50**, 6872–6874 (2014)
35. A. Dhakshinamoorthy, M. Alvaro, H. Garcia, Aerobic oxidation of styrenes catalyzed by an iron metal organic framework. ACS Catal. **1**, 836–840 (2011)
36. A. Dhakshinamoorthy, M. Alvaro, H. Garcia, Aerobic oxidation of thiols to disulfides using iron metal-organic frameworks as solid redox catalysts. Chem. Commun. **46**, 6476–6478 (2010)
37. A. Dhakshinamoorthy, M. Alvaro, H. Garcia, Metal-organic frameworks as efficient heterogeneous catalysts for the regioselective ring opening of epoxides. Chem. - A Eur. J. **16**, 8530–8536 (2010)
38. K. Momma, F. Izumi, VESTA : a three-dimensional visualization system for electronic and structural analysis. J. Appl. Crystallogr. **41**, 653–658 (2008)
39. A. Dhakshinamoorthy, M. Alvaro, P. Horcajada, E. Gibson, M. Vishnuvarthan, A. Vimont, J.M. Grenèche, C. Serre, M. Daturi, H. Garcia, Comparison of porous iron trimesates basolite F300 and MIL-100(Fe) as heterogeneous catalysts for lewis acid and oxidation reactions: roles of structural defects and stability. ACS Catal. **2**, 2060–2065 (2012)
40. H. Leclerc, A. Vimont, J.-C. Lavalley, M. Daturi, A.D. Wiersum, P.L. Llwellyn, P. Horcajada, G. Férey, C. Serre, Infrared study of the influence of reducible iron(iii) metal sites on the adsorption of CO, CO2, propane, propene and propyne in the mesoporous metal–organic framework MIL-100. Phys. Chem. Chem. Phys. **13**, 11748 (2011)
41. J.W. Yoon, Y.K. Seo, Y.K. Hwang, J.S. Chang, H. Leclerc, S. Wuttke, P. Bazin, A. Vimont, M. Daturi, E. Bloch, P.L. Llewellyn, C. Serre, P. Horcajada, J.M. Grenèche, A.E. Rodrigues, G. Férey, Controlled reducibility of a metal-organic framework with coordinatively unsaturated sites for preferential gas sorption. Angew. Chemie - Int. Ed. **49**, 5949–5952 (2010)
42. B.-J. Zhu, X.-Y. Yu, Y. Jia, F.-M. Peng, B. Sun, M.-Y. Zhang, T. Luo, J.-H. Liu, X.-J. Huang, Iron and 1,3,5-benzenetricarboxylic metal-organic coordination polymers prepared by solvothermal method and their application in efficient As(V) removal from aqueous solutions. J. Phys. Chem. C **116**, 8601–8607 (2012)
43. Y.K. Seo, J.W. Yoon, J.S. Lee, U.H. Lee, Y.K. Hwang, C.H. Jun, P. Horcajada, C. Serre, J.S. Chang, Large scale fluorine-free synthesis of hierarchically porous iron(III) trimesate MIL-100(Fe) with a zeolite MTN topology. Microporous Mesoporous Mater. **157**, 137–145 (2012)
44. K. Guesh, C.A.D. Caiuby, Á. Mayoral, M. Díaz-García, I. Díaz, M. Sanchez-Sanchez, Sustainable Preparation of MIL-100(Fe) and Its Photocatalytic Behavior in the Degradation of Methyl Orange in Water. Cryst Growth Des (2017). https://doi.org/10.1021/acs.cgd.6b01776
45. L. Sciortino, A. Alessi, F. Messina, G. Buscarino, F.M. Gelardi, Structure of the FeBTC Metal-Organic Framework: A Model Based on the Local Environment Study. J. Phys. Chem. C **119**, 7826–7830 (2015)
46. V.P. Santos, T.A. Wezendonk, J.J.D. Jaén, A.I. Dugulan, M.A. Nasalevich, H.U. Islam, A. Chojecki, S. Sartipi, X. Sun, A.A. Hakeem, A.C.J. Koeken, M. Ruitenbeek, T. Davidian, G.R. Meima, G. Sankar, F. Kapteijn, M. Makkee, J. Gascon, Metal organic framework-mediated synthesis of highly active and stable Fischer-Tropsch catalysts. Nat. Commun. (2015). https://doi.org/10.1038/ncomms7451
47. M.L. Farquhar, J.M. Charnock, F.R. Livens, D.J. Vaughan, Mechanisms of arsenic uptake from aqueous solution by interaction with goethite, lepidocrocite, mackinawite, and pyrite: an x-ray absorption spectroscopy study. Environ. Sci. Technol. **36**, 1757–1762 (2002)
48. S. Surblé, F. Millange, C. Serre, G. Férey, R.I. Walton, An EXAFS study of the formation of a nanoporous metal–organic framework: evidence for the retention of secondary building units during synthesis. Chem. Commun. (2006). https://doi.org/10.1039/B600709K
49. R.K. Dhar, Y. Zheng, J. Rubenstone, A. Van Geen, A rapid colorimetric method for measuring arsenic concentrations in groundwater. Anal. Chim. Acta **526**, 203–209 (2004)
50. V. Lenoble, Arsenite oxidation and arsenate determination by the molybdene blue method. Talanta **61**, 267–276 (2003)
51. N. Jain, H.C. Joshi, S.C. Dutta, S. Kumar, H. Pathak, Biosorption of copper from wastewater using jatropha seed coat. J. Sci. Indust. Res. **67**, 154–160 (2008)
52. S. Ayoob, A.K. Gupta, P.B. Bhakat, Performance evaluation of modified calcined bauxite in the sorptive removal of arsenic(III) from aqueous environment. Coll. Surf. A Physicochem. Eng. Asp. **293**, 247–254 (2007)
53. T. Basu, K. Gupta, U.C. Ghosh, Equilibrium and thermodynamics on arsenic (III) sorption reaction in the presence of background ions occurring in groundwater with nanoparticle agglomerates of hydrous iron (III) + chromium (III) mixed oxide †. J. Chem. Eng. Data. (2010). https://doi.org/10.1021/je901010x
54. B. Ravel, M. Newville, ATHENA, ARTEMIS, HEPHAESTUS: Data analysis for X-ray absorption spectroscopy using IFEFFIT. J. Synchrotron Radiat. **12**, 537–541 (2005)
55. Y. Gu, D. Xie, Y. Wang, W. Qin, H. Zhang, G. Wang, Y. Zhang, H. Zhao, Facile fabrication of composition-tunable Fe/Mg bimetal-organic frameworks for exceptional arsenate removal. Chem. Eng. J. **357**, 579–588 (2019)
56. J. Cai, X. Mao, W.-G. Song, Adsorption behavior and structure transformation of mesoporous metal–organic frameworks towards arsenates and organic pollutants in aqueous solution. Mater. Chem. Front. **2**, 1389–1396 (2018)

57. C. Wang, X. Liu, J.P. Chen, K. Li, Superior removal of arsenic from water with zirconium metal-organic framework UiO-66. Sci. Rep. **5**, 1–10 (2015)
58. V. Gascón, M.B. Jiménez, R.M. Blanco, M. Sanchez-Sanchez, Semi-crystalline Fe-BTC MOF material as an efficient support for enzyme immobilization. Catal. Today **304**, 119–126 (2018)
59. A. Jain, S.P. Ong, G. Hautier, W. Chen, W.D. Richards, S. Dacek, S. Cholia, D. Gunter, D. Skinner, G. Ceder, K.A. Persson, Commentary: The materials project: a materials genome approach to accelerating materials innovation. APL Mater. doi **10**(1063/1), 4812323 (2013)